Optical Materials 33 (2011) 308–314

Contents lists available at ScienceDirect

Optical Materials

journal homepage: www.elsevier.com/locate/optmat

Optical properties of Mn-doped ZnS semiconductor nanoclusters synthesized by a hydrothermal process

Tran Thi Quynh Hoa [a], Ngo Duc The [b], Stephen McVitie [b], Nguyen Hoang Nam [a], Le Van Vu [a], Ta Dinh Canh [a], Nguyen Ngoc Long [a,*]

[a] Faculty of Physics, Hanoi University of Science, 334 Nguyen Trai Road, Thanh Xuan District, Hanoi, Viet Nam
[b] Department of Physics and Astronomy, University of Glasgow, Glasgow G12 8QQ, Scotland, United Kingdom

ARTICLE INFO

Article history:
Received 1 March 2010
Received in revised form 6 August 2010
Accepted 14 September 2010
Available online 13 October 2010

Keywords:
Optical properties
Nanocluster
Hydrothermal method
Mn-doped ZnS

ABSTRACT

Undoped and Mn-doped ZnS nanoclusters have been synthesized by a hydrothermal approach. Various samples of the ZnS:Mn with 0.5, 1, 3, 10 and 20 at.% Mn dopant have been prepared and characterized using X-ray diffraction, energy-dispersive analysis of X-ray, high resolution electron microscopy, UV–vis diffusion reflection, photoluminescence (PL) and photoluminescence excitation (PLE) measurements. All the prepared ZnS nanoclusters possess cubic sphalerite crystal structure with lattice constant $a = 5.408 \pm 0.011$ Å. The PL spectra of Mn-doped ZnS nanoclusters at room temperature exhibit both the 495 nm blue defect-related emission and the 587 nm orange Mn^{2+} emission. Furthermore, the blue emission is dominant at low temperatures; meanwhile the orange emission is dominant at room temperature. The Mn^{2+} ion-related PL can be excited both at energies near the band-edge of ZnS host (the UV region) and at energies corresponding to the Mn^{2+} ion own excited states (the visible region). An energy schema for the Mn-doped ZnS nanoclusters is proposed to interpret the photoluminescence behaviour.

1. Introduction

Since the first report of Mn-doped ZnS semiconductor nanocrystals [1,2], many studies on doped semiconductor nanoparticles appeared. Among them, doped II-VI semiconductor nanocrystals have attracted a great deal of attention, including CdS:Mn [3–5], CdS:Eu [6], ZnO:Co,Ni [7], ZnSe:Mn [8], ZnS:Cu [9,10], ZnS:Pb,Cu [11] and ZnS:Mn [12–20]. ZnS, an important II-VI semiconductor, has attracted enormous attention because it has been commercially used for a variety of applications such as electroluminescent devices, solar cells and other optoelectronic devices. In addition, ZnS is suitable for use as a host material for a variety of dopants because of its wide band gap. It was reported by Bhargava et al. [1] that the doping with Mn into ZnS nanocrystals results in the luminescent efficiency enhancement and the lifetime shorting in comparison with that of the bulk material. These results were explained on the basis of the interaction of the *sp* electron hole of the host (ZnS) and the 3*d* electrons of the impurity (Mn) under condition of the quantum confinement for the *sp* states. Analysing photoluminescence excitation (PLE) spectra in the ultraviolet- and visible-regions for the ZnS:Mn nanoparticle samples with different sizes, Tanaka [5] and Chen et al. [20] proposed a model for the energy transfer from the host ZnS lattice to Mn^{2+} *d* levels. It was concluded [5] that the Mn^{2+} luminescence under the interband excitation occurs mostly by the energy transfer from the electron–hole pairs delocalized inside the ZnS host nanocrystals.

In this work we synthesized Mn-doped ZnS nanoclusters with different Mn concentrations using a hydrothermal approach. Low temperature hydrothermal synthesis (between 150–250 °C) is becoming popular because of low-cost facility, capability of large-scale preparation of materials and environmental friendliness. On the other hand, by controlling temperature, pressure, reaction time, precursor chemicals and solvent, one can get various morphology, dimensions and structure of the final products.

In order to find out about the emission behaviour of the Mn-doped ZnS nanoclusters, photoluminescence (PL) and photoluminescence excitation (PLE) spectra were investigated in wide temperature range from 10 to 300 K. The Mn^{2+} ion-related photoluminescence can be excited both at energies near the band-edge of ZnS host (the UV region) and at energies corresponding to the Mn^{2+} ion own excited states (the visible region). These results allowed clearing up the mechanism of energy transfer to the Mn^{2+} ion. A model of emission centers in the Mn-doped ZnS nanoclusters was proposed to explain the observed luminescence behaviour.

2. Experimental

2.1. Synthesis of Mn-doped ZnS nanoclusters

All the chemicals used in our experiment, including zinc acetate $Zn(CH_3COO)_2{\cdot}2H_2O$, manganese acetate $Mn(CH_3COO)_2{\cdot}2H_2O$ and

* Corresponding author.
E-mail address: longnn@vnu.edu.vn (N.N. Long).

0925-3467/$ - see front matter © 2010 Elsevier B.V. All rights reserved.
doi:10.1016/j.optmat.2010.09.008

thiourea NH_2CSNH_2 are of analytic grade without further purification. The nanoclusters of ZnS:Mn have been synthesized under hydrothermal conditions. The procedure was as follows: first, 16.46 g $Zn(CH_3COO)_2{\cdot}2H_2O$ and 1.34 g $Mn(CH_3COO)_2{\cdot}2H_2O$ were completely dissolved into de-ionized water to obtain 0.25 M aqueous solutions, respectively. 19.98 g NH_2CSNH_2 was dissolved into de-ionized water, forming 0.75 M aqueous solution. Second, appropriate amounts of 0.25 M solution of zinc acetate and 0.25 M solution of manganese acetate were mixed to get 50 mL of the mixture solution. Then 50 mL of 0.75 M solution of thiourea was added into the above mixture solution, followed by steady stirring for 30 min. The last mixture solution was placed in sealed Teflon-lined autoclave with 120 mL capacity. The closed autoclave was placed inside a box furnace at a preset temperature of 200 °C for 24 h and then cooled to room temperature naturally. The resulting precipitate was filtered off and washed 10 times in water. The final product was dried in air at 60 °C for 12 h. The Mn doping ratio in the synthesized ZnS samples was 0, 0.5, 1, 3, 10 and 20 at.%.

2.2. Characterization of the samples

Crystal structure of the nanoclusters was analysed by using an X-ray diffractometer (SIEMENS D5005, Bruker, Germany) with Cu–$K_{\alpha 1}$ (λ = 1.54056 Å) irradiation. The composition of the samples was determined by an energy-dispersive X-ray (EDX) spectrometer (EDS, OXFORD ISIS 300) attached to the JEOL-JSM 5410 LV scanning electron microscope. The morphology of the samples was characterized by using a high resolution transmission electron microscope (HRTEM) (FEI Tecnai TF20 FEG TEM). Diffuse reflection spectroscopy measurements were carried out on a UV–VIS-NIR Cary-5G spectrophotometer. The spectra were recorded at room temperature in the wavelength region of 200–900 nm. Absorption spectra of the samples were obtained from the diffuse reflectance values by using the Kubelka–Munk function [21]:

$$F(R) = \frac{(1-R)^2}{2R} = \frac{K}{S} \quad (1)$$

where R, K and S are the reflection, the absorption and the scattering coefficient, respectively. The PL and the PLE spectra were measured in the range of temperatures from 10 up to 300 K were carried out on a spectrofluorometer (Fluorolog FL 3-22 Jobin Yvon Spex, USA) with a 450 W xenon lamp as an excitation source.

3. Results and discussion

3.1. Structure characterization and morphology

Typical X-ray diffraction (XRD) patterns for the undoped ZnS nanoclusters and the ZnS:Mn nanoclusters doped with various Mn contents (0.5, 1, 3, 10 and 20 at.%) are shown in Fig. 1, where the diffraction peaks at 2θ values of 28.5°, 33.1°, 47.5° and 56.4° correspond to the (1 1 1), (2 0 0), (2 2 0) and (3 1 1) diffraction planes. All the peaks in the XRD patterns clearly indicate that the undoped ZnS and Mn-doped ZnS nanoclusters possess cubic sphalerite crystal structure. No other diffraction peaks are detected except for the ZnS related peaks. These results are in agreement with those of other authors [13,16].

The lattice constant determined from the XRD patterns is a = 5.408 ± 0.011 Å, which is close to the reported value of cubic ZnS (JCPDS card, No. 05-0566, a = 5.4060 Å). The average sizes of the ZnS nanocrystals were estimated by Debye–Scherrer's formula [22]:

$$L = \frac{0.9\lambda}{\beta \cos\theta} \quad (2)$$

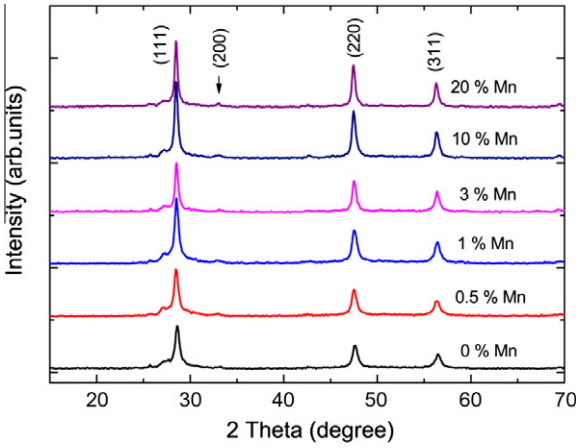

Fig. 1. Typical XRD patterns for the samples of the undoped ZnS and the Mn-doped ZnS with various Mn contents.

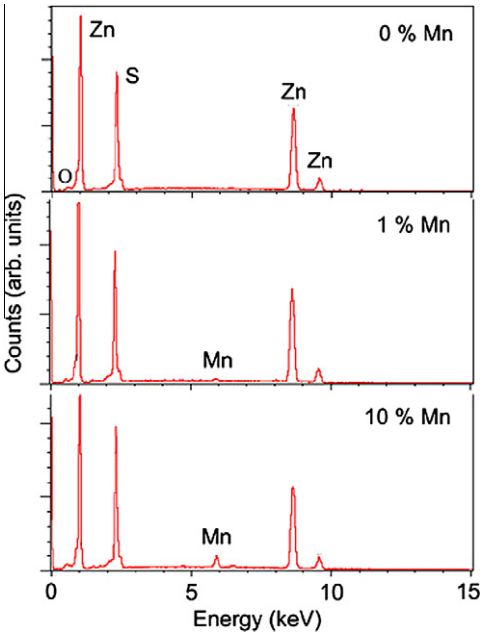

Fig. 2. Typical EDX spectra of the undoped ZnS and the ZnS nanoclusters doped with 1 and 10 at.% Mn.

where β is the full width at half maximum (FWHM) in radians of the diffraction peaks, θ is the Bragg's diffraction angle and λ is the wavelength for the $K_{\alpha 1}$ component of the employed copper radiation (1.54056 Å). The calculated sizes of the ZnS nanocrystals were found to be 13.8, 13.8, 14.4, 18.3, 18.6 and 21.7 nm for the samples with Mn contents of 0, 0.5, 1, 3, 10 and 20 at.%, respectively.

The EDX spectrum measurements showed that EDX spectra of all the Mn-doped ZnS samples exhibit the peaks related to elemental Mn. Representative EDX spectra of the undoped ZnS and the ZnS nanoclusters doped with 0.5 and 10 at.% Mn are shown in Fig. 2. In pure ZnS, elemental Zn and S were found in a near-stoichiometric ratio with little sulfur deficiency (Zn: 51.7, S: 48.3 at.%). In the Mn-doped ZnS nanoclusters, the peaks related to elemental Mn can be seen already in 0.5 at.% Mn-doped sample as seen from Fig. 2. The amount of Mn obtained by EDX analysis in 0.5 and 10 at.% doped ZnS samples was 0.59 and 2.06 at.%, respectively. It is noted that a small amount of oxygen was still observed in the EDX spectra.

Fig. 3(a) shows a typical HRTEM image of the 1 at.% Mn-doped ZnS nanoclusters. The selected area electron diffraction (SAED) pattern of this sample is shown in the inset of Fig. 3(a). As seen from the picture, the SAED pattern shows a set of rings corresponding to diffraction from different planes of the nanocrystallites instead of spots due to the random orientation of the crystallites. It is evidently observed three rings corresponding to the (1 1 1), (2 2 0) and (3 1 1) lattice planes of the cubic phase of ZnS, which is in good agreement with the above XRD patterns. Fig. 3(b) represents a magnified HRTEM image of the 1 at.% Mn-doped ZnS with the (1 1 1) lattice planes. The spacing of the lattice fringes in the HRTEM image is found to be 3.12 Å, which corresponds to the (1 1 1) plane of the cubic phase of ZnS. This is also confirmed from the fast Fourier transform (FFT) pattern of the HRTEM image, as shown in the inset of Fig. 3(b).

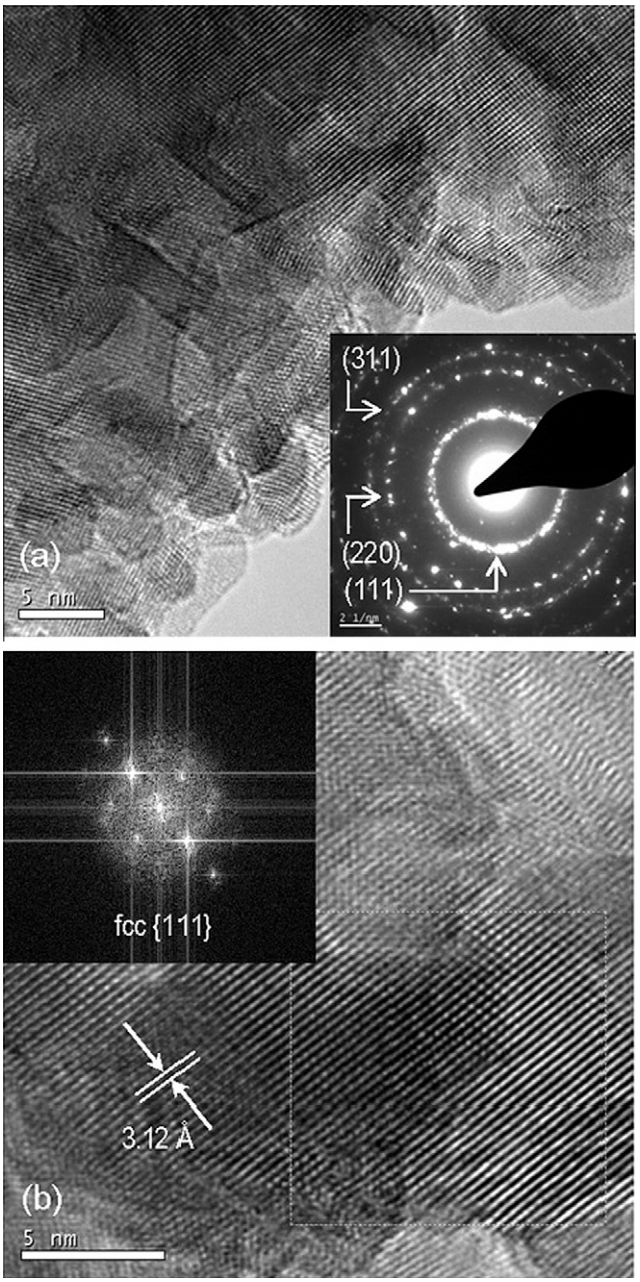

Fig. 3. (a) Typical HRTEM image of the 1 at.% Mn-doped ZnS nanoclusters, (b) magnified HRTEM image of the 1 at.% Mn-doped ZnS with the (1 1 1) lattice planes. SAED and FFT patterns are shown in the insets of figures (a) and (b), respectively.

3.2. Absorption and photoluminescence properties

Fig. 4 depicts reflection spectra of the undoped ZnS and the Mn-doped ZnS nanoclusters measured at room temperature by a diffuse reflection technique. It is noted that the absorption edges of the ZnS:Mn nanoclusters show a minor shift with increasing the Mn concentration. Additionally, it is interesting to note that five absorption bands located at 3.171, 2.898, 2.668, 2.504 and 2.318 eV were first time clearly observed from the reflection spectra of the 3, 10 and 20 at.% Mn-doped ZnS samples. These five absorption bands can be assigned to the transitions from the $^6A_1(^6S)$ ground state to the $^4E_2(^4D)$; $^4T_2(^4D)$; $^4E(^4G)$, $^4A1(^4G)$; $^4T_2(^4G)$ and $^4T_1(^4G)$ excited states of the Mn^{2+} ion, respectively, because their energies are in good agreement with those of the excited states of the Mn^{2+} ion in ZnS:Mn bulk crystal [19,23].

Room temperature absorption spectra of the ZnS samples obtained from the diffuse reflectance values by using the Kubelka–Munk function $F(R)$ are shown in Fig. 5. All the spectra exhibit a sharp absorption edge and an onset of absorption at 3.5–3.6 eV. The inset of Fig. 5 obviously shows five absorption bands related to the optical transitions within Mn^{2+} ion in the spectra of the 3, 10 and 20 at.% Mn-doped ZnS samples.

It is well known that cubic ZnS is a direct-gap semiconductor [24]. The relation between the absorption coefficients (α) and the incident photon energy ($h\nu$) for the case of allowed direct transition is written as follows [25]:

$$\alpha h\nu = A(h\nu - E_g)^{1/2} \tag{3}$$

where A is a constant and E_g is the bandgap of the material. The plots of $[F(R) \times h\nu]^2$ versus $h\nu$ for the undoped ZnS and the Mn-doped ZnS nanoclusters are represented in Fig. 6. By extrapolating the straight portion of the graph on $h\nu$ axis at $\alpha = 0$ we found the bandgaps of the undoped ZnS and the Mn-doped ZnS nanoclusters with the concentration of 0.5, 1, 3, 10 and 20 at.% to be 3.578, 3.588, 3.598, 3.544, 3.512 and 3.503 eV, respectively. These values can be compared with the bandgap values of 3.5–3.7 eV at room temperature for the sphalerite bulk ZnS [26]. From Fig. 6, it is noted that the absorption edge is slightly shifted toward the high energy side with increasing the Mn concentration up to 1 at.%. Then the band gap is found to decrease for increased Mn concentrations of 3, 10, and 20 at.% as seen from the inset of Fig. 6.

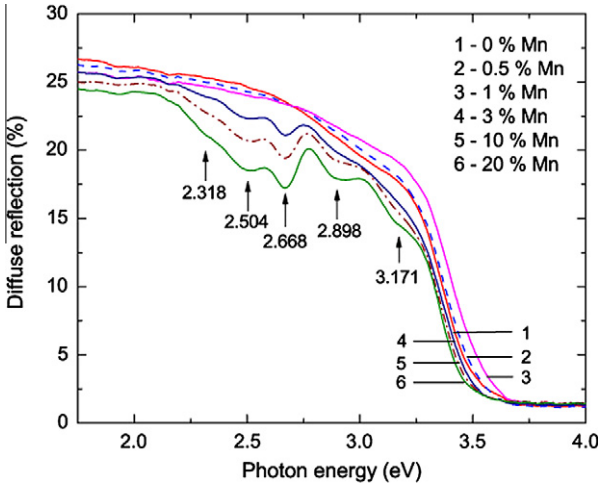

Fig. 4. Diffuse reflection spectra at room temperature of the undoped ZnS and the Mn-doped ZnS nanoclusters. Five absorption bands related to the optical transitions within Mn^{2+} ion are clearly observed in the spectra of the 3, 10 and 20 at.% Mn-doped ZnS samples.

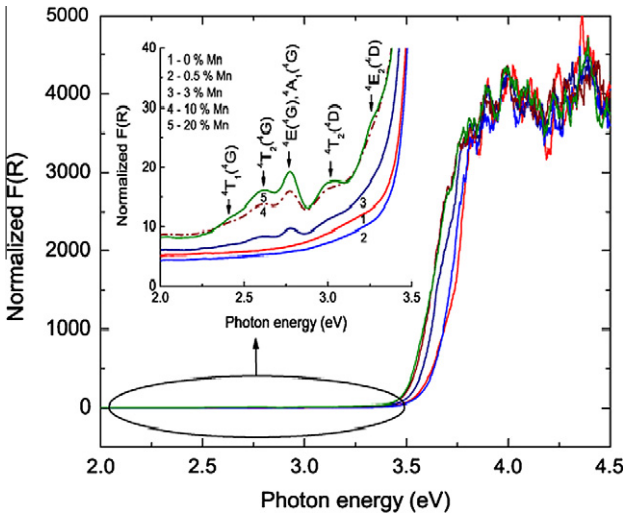

Fig. 5. Plots of F(R) versus photon energy for the undoped ZnS and the Mn-doped ZnS nanoclusters. The inset shows five absorption bands related to the optical transitions within Mn^{2+} ion in the spectra of the 3, 10 and 20 at.% Mn.

The the same shifts of the absorption edge with increasing the Mn concentration from 0 to 9 at.% at a fixed size of ZnS nanoclusters were reported in references [16,17]. Interestingly, this variation of the band gap with Mn concentration is the opposite of what is observed in the case of Mn-doped CdS nanoclusters [27], where it was reported that a minimum in the band-gap energy was observed for about 5–8% Mn concentration. These changes of the band gap with Mn concentration have been ascribed to the sp-3d exchange interaction in a confined regime.

In our case, the sizes of the ZnS nanocrystals were found to be in the range of 13.8–21.7 nm which are larger than the exciton Bohr radius (~2.1 nm) in a cubic ZnS. Hence the slight shrinkage of band gap may be assigned to the weak quantum confinement effect in our ZnS clusters.

We have measured PL spectra of the ZnS samples at room temperature under the 250, 325, 355, 362, 432 and 469 nm excitation wavelengths.

Fig. 7 shows the PL spectra at room temperature excited with the wavelength of 362 nm (3.425 eV) for the undoped ZnS nanoclusters and the ZnS nanoclusters doped with various Mn dopant concentrations. It is found that the PL spectra of the undoped samples show only one blue emission band centered at 490 nm, which could be usually assigned to radiative recombination involving defect states in the ZnS nanocrystals [28,29]. For all the doped samples, two emission bands are observed in the PL spectra. One is a weak blue emission band located at 490 nm and another is a dominant orange emission band peaked at 588 nm. The 588 nm emission band was attributed to the $^4T_1(^4G) \rightarrow {}^6A_1(^6S)$ transition within the 3*d* shell of Mn^{2+} ion [1]. Additionally, it is found from Fig. 7 that the $^4T_1(^4G) \rightarrow {}^6A_1(^6S)$ emission intensity shows a maximum when the Mn doping content is 1 at.%, which is in good agreement with previous reports [30–32]. It is noticed that the area under the luminescence spectra reaches to a maximum at Mn^{2+} concentrations of 0.5 and 1 at.%, which demonstrates indirectly that the luminescence quantum efficiency of our samples increases to a maximum when doping the samples with these concentration of Mn.

The sharp fall in intensity of the Mn^{2+} emission for the 3, 10 and 20 at.% Mn-doped ZnS samples can be attributed to the concentration quenching effect due to the pairing or coagulation of the Mn ions.

It must be noted that the PL spectra at room temperature under the 250, 325 and 355 nm excitations (not shown here) have the same form as the PL spectrum excited with the 362 nm wavelength. On the contrary, the PL spectra at room temperature under the 432 and 469 nm excitations exhibit only the Mn^{2+} ion emission. The fact that both the 490 nm blue and the 588 nm orange emission bands are simultaneously observed in the PL spectra of the Mn-doped ZnS nanoclusters proves that the Mn^{2+} ions were indeed incorporated within the ZnS nanocrystals as noted in previous report [33].

In order to clear the nature of the emission bands, we have recorded PLE spectra at room temperature. The PLE spectra monitored at the 495 nm emission band at room temperature for all the ZnS samples are depicted in Fig. 8(a). From this figure, it is possible to infer that the 495 nm emission band related to the defect states can be excited by the near-band-edge energies (the UV region). The PLE spectra monitored at the 587 nm emission band at room temperature for the ZnS samples are illustrated in Fig. 8(b). For the undoped ZnS nanoclusters, the PLE spectra monitored at the 587 nm emission band involve only one near-band-edge absorption band centered at 363 nm (line 1 in Fig. 8(b)). On the contrary, for all the Mn-doped ZnS nanoclusters, the PLE spectra monitored at the 587 nm wavelength exhibit both the near-band-edge absorption band and five absorption bands peaked at

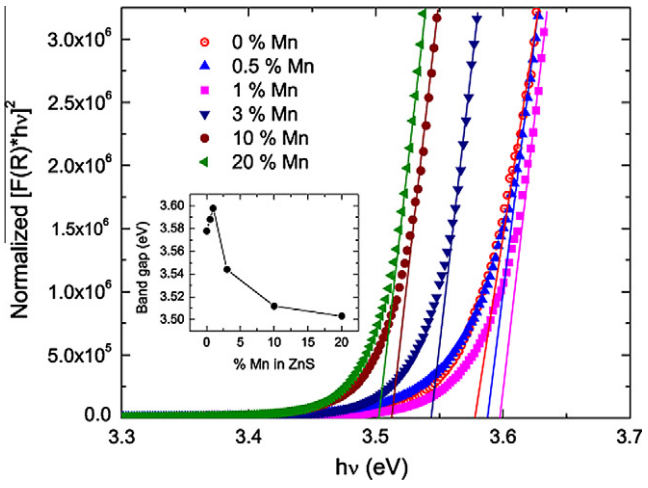

Fig. 6. The plots of $[F(R) \times h\nu]^2$ versus $h\nu$ for the undoped ZnS and the Mn-doped ZnS nanoclusters. The shift of absorption edge of the ZnS nanoclusters as a function of Mn concentration is shown in the inset.

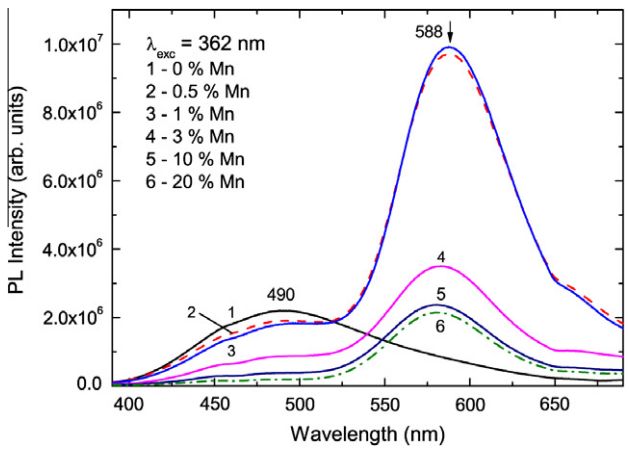

Fig. 7. PL spectra at room temperature under the 362 nm excitation wavelength for the undoped ZnS nanoclusters and the ZnS nanoclusters doped with different Mn dopant concentrations.

391 nm (3.17 eV), 432 nm (2.87 eV), 467 nm (2.65 eV), 500 nm (2.48 eV) and 532 nm (2.33 eV).

The PLE spectra for the 1 at.% Mn-doped ZnS nanoclusters have been measured in the temperature range of 10–300 K. It was noticed that the PLE spectra monitored at the 495 nm and the 587 nm emission bands at low temperatures (not shown here) exhibited the same shape as those at room temperature (Fig. 8).

The energy positions of the above mentioned five bands are in good agreement with the energies of the excited states of the Mn^{2+} ion in ZnS:Mn bulk crystal [19,23]. Therefore, the five absorption bands at 391, 432, 467, 500 and 532 nm are attributed to the $^6A_1(^6S) \rightarrow {}^4E_2(^4D)$; $^6A_1(^6S) \rightarrow {}^4T_2(^4D)$; $^6A_1(^6S) \rightarrow {}^4E(^4G)$, $^4A_1(^4G)$; $^6A_1(^6S) \rightarrow {}^4T_2(^4G)$ and $^6A_1(^6S) \rightarrow {}^4T_1(^4G)$ transitions within Mn^{2+} ion, respectively. The doublet at 467 nm in the PLE spectra shown in Fig. 8(b) may be attributed to the other excitation mechanism related to stacking faults.

The PL spectra of the 1 at.% Mn-doped ZnS sample have been measured in the range of temperatures from 10 K to room temperature. In Fig. 9 are shown the PL spectra of this sample at some temperatures under the 362 nm excitation. The PL spectra exhibit two emission bands: the blue band attributed to the defect states and the orange band assigned to Mn^{2+} ion. In addition, the blue band is dominant at low temperatures, the orange band is dominant at high temperatures. Like the PL spectra at room temperature, those at low temperatures under the 432 and 469 nm excitations exhibit only the orange emission relating to Mn^{2+} ion.

Temperature dependence of the peak position and the peak intensity for the defect-related blue and Mn^{2+} emissions in the

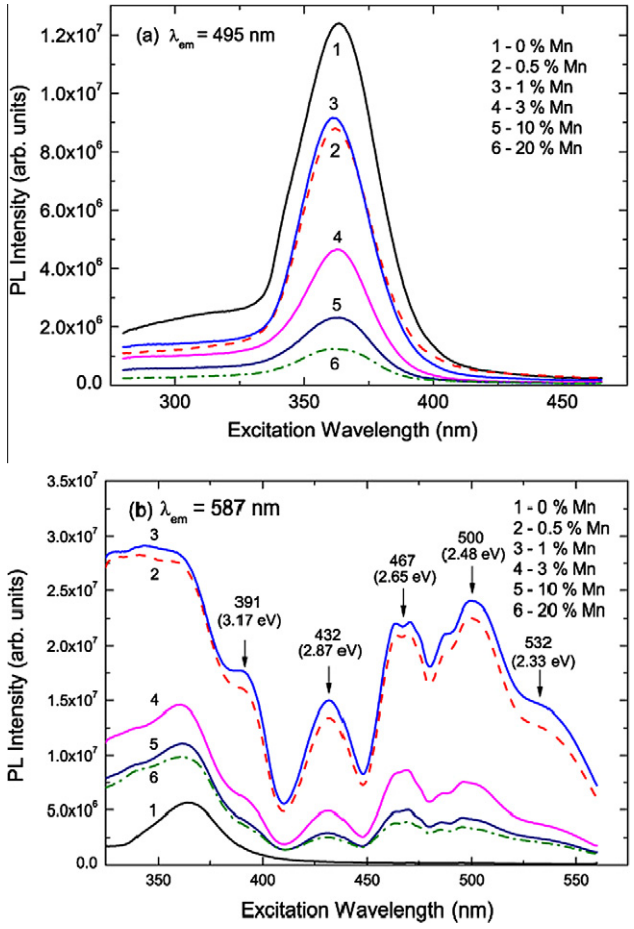

Fig. 8. PLE spectra monitored at (a) the 495 nm and (b) the 587 nm emission peaks at room temperature of the ZnS samples.

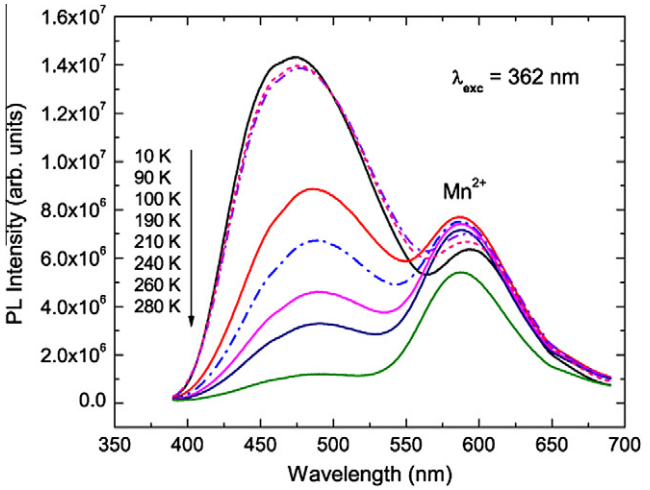

Fig. 9. PL spectra of the 1 at.% Mn-doped ZnS sample at some temperatures under the 362 nm excitation.

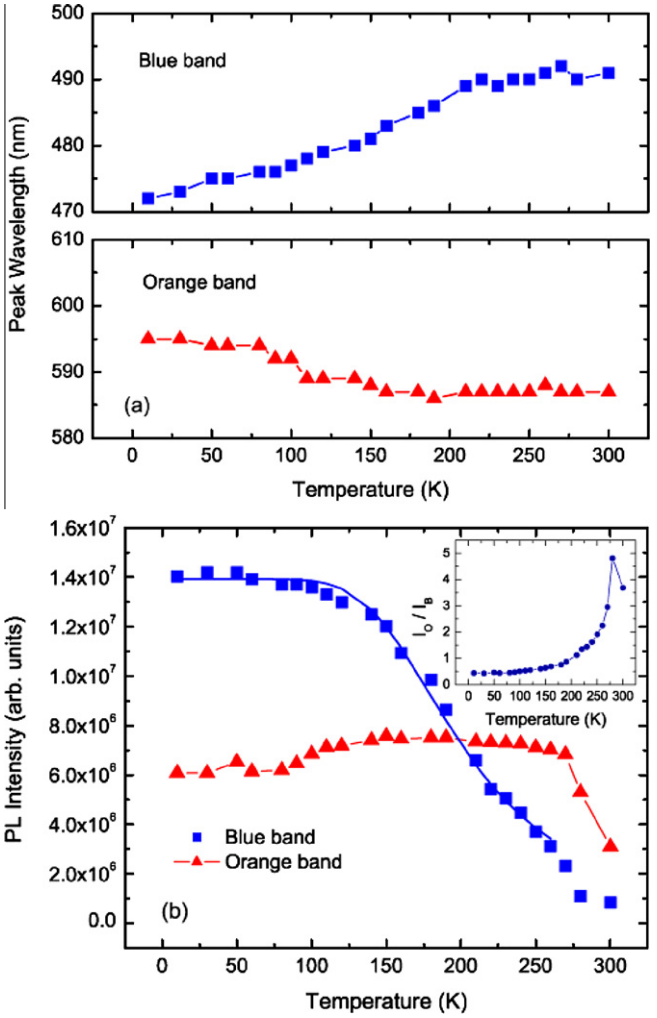

Fig. 10. Temperature dependence of (a) peak position and (b) peak intensity for the defect-related blue and Mn^{2+} emissions in the 1 at.% Mn-doped ZnS nanoclusters. Intensity ratio of the orange and the blue peaks I_O/I_B as a function of temperature is shown in the inset.

1 at.% Mn-doped ZnS nanoclusters is displayed in Fig. 10. As the temperature increases in the range from 10 to 300 K, the blue

emission band shifts by 19 nm to the longer wavelength. On the contrary, the Mn^{2+} emission band shifts by 7 nm to the shorter wavelength with increasing temperature as seen from Fig. 10(a).

The blue emission band shows a strong decrease in intensity with increasing temperature (Fig. 10(b)). According to the theory of thermal quenching, the temperature dependence of the emission intensity, $I(T)$, can be described by the following expression [20]:

$$I(T) = \frac{I_0}{1 + A\exp\left(-\frac{E}{kT}\right)} \quad (4)$$

where E is the activation energy, k is the Boltzmann's constant, A is a constant and I_0 is the emission intensity at 0 K. The solid line in Fig. 10(b) shows the calculated result using the above formula with the following parameters: $I_0 = (1.39 \pm 0.03) \times 10^7$ (arb. units), $A = (170 \pm 75)$ (arb. units) and $E = (90 \pm 7)$ meV. These values are in agreement with those from previous report [20] for the 430 nm emission peak in ZnS:Mn nanoparticles. The blue luminescence band is shifted to the low-energy side with increasing temperature. This emission band can be interpreted as a donor–acceptor pair (DAP) emission. Indeed, it is known that the DAP emission energy is described as follows [34]:

$$h\nu_{DA} = E_g - (E_D + E_A) + \frac{q^2}{\varepsilon r} \quad (5)$$

where q is the electrical charge of the acceptor and the donor ions, ε is the dielectric constant, r is the distance between the donor and the acceptor, E_g is the band gap and E_D and E_A are the donor and the acceptor binding energies when $r = \infty$, respectively.

The photon energy $h\nu_{DA}$ emitted from DAPs is demonstrated in Fig. 11. As seen from this figure, the DAPs with small distance r are responsible for the high-energy part of the DAP emission band. With increasing temperature, carriers on the DAPs with small distance r are thermally released into the bands, which results in extinguishing the high-energy part of the DAP emission band, therefore the band peak is shifted to the low-energy side and its intensity decreases as observed in our experiment.

As mentioned above, the intensity of the DAP emission was remarkably reduced with increasing temperature, whereas the intensity of Mn^{2+} emission was weakly dependent on temperature in the range of 10–270 K, which is consistent with previous reports [20,35] for the case of ZnS:Mn nanocrystals. However, unlike the results reported in [20,35], where the intensity of the Mn^{2+} emission was slightly decreased as the temperature increased, in our case the Mn^{2+} emission intensity kept constant in the temperature range of 10–80 K, was somewhat increased in the range of 80–140 K and then kept again constant in the range of 140–270 K (Fig. 10(b)). The intensity ratio of the orange and the blue peaks I_O/I_B shown in the inset of Fig. 10(b) remarkably increases when the temperature is increased.

Based on the energy schema depicted in Fig. 11, the observed photoluminescent behaviour of the Mn-doped ZnS nanoclusters can be interpreted. On the one hand, the Mn^{2+} ion-related PL can be excited at energies corresponding to the Mn^{2+} ion own excited states. On the other hand, when the Mn-doped ZnS nanoclusters are excited by UV light (interband transitions), electrons in the valence band of the ZnS host absorb the photon energy and transfer to the conduction band, generating free electrons in the conduction band and free holes in the valence band. At low temperatures most of these photogenerated electrons and holes are trapped on the DAP states (transition (1)) and then recombine via these states, exhibiting the dominant blue emission. A number of the photogenerated holes in the valence band are trapped by Mn^{2+} ions which then become Mn^{3+} ions. Subsequent trapping of a number of the photogenerated electrons in the conduction band results in Mn^{2+} ions in an excited state $(Mn^{2+})^*$ (transition (2)) and the following transitions of Mn ions from the excited state $(Mn^{2+})^*$ to the basic state Mn^{2+} accompany the orange emission. This process can be described by the following equations [36]:

$$\begin{aligned} &Mn^{2+} + h^+(VB) \rightarrow Mn^{3+} \\ &Mn^{3+} + e^-(CB) \rightarrow (Mn^{2+})^* \\ &(Mn^{2+})^* \rightarrow Mn^{2+} + h\nu_{Mn} \end{aligned} \quad (6)$$

With increasing temperature, electrons and holes on the DAPs with smaller distance r are thermally released into the bands. A part of the holes and the electrons just released from the DAPs are retrapped by Mn^{2+} ions (transition (3) in Fig. 11), emitting the orange photon. The result is that the blue emission strongly quenches, on the contrary, the intensity of the Mn^{2+} emission not only does not decrease, but even can somewhat increase with increasing temperature as observed in our ZnS:Mn samples. It is noted that in our ZnS:Mn samples, the Mn^{2+} ion is not excited via the DAPs, because if this occurs, the intensity of both the blue and the orange emissions will decrease with increasing temperature, which is not consistent with our experimental observation.

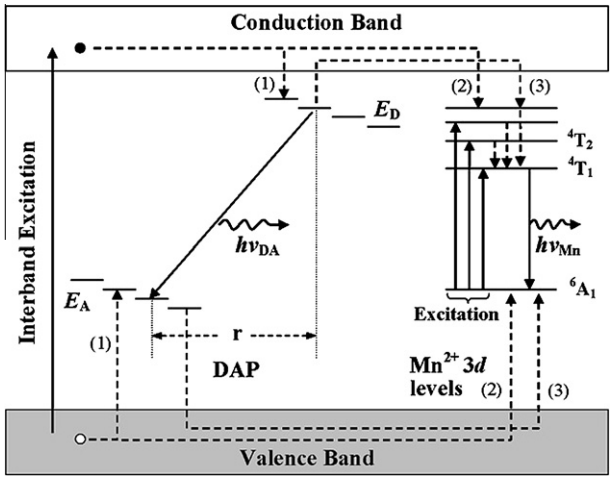

Fig. 11. Schematic representation of the proposed mechanism for the PL excitation, the energy transfer and the PL in ZnS:Mn nanoclusters.

4. Conclusion

Undoped and Mn-doped ZnS nanoclusters with 0.5, 1, 3, 10 and 20 at.% Mn dopant have been prepared by a hydrothermal approach. All the prepared ZnS nanoclusters possessed cubic sphalerite crystal structure with lattice constant $a = 5.408 \pm 0.011$ Å. The absorption bands corresponding to the transitions from the basic state to the excited states of the Mn^{2+} ion were observed in both the reflection, absorption spectra and the PLE spectra. The PL spectra of Mn-doped ZnS nanoclusters exhibited both the blue defect-related emission and the orange Mn^{2+} ion-related emission. Furthermore, the blue emission was dominant at low temperatures; meanwhile the orange emission was dominant at room temperature. The Mn^{2+} emission intensity showed a maximum when the Mn doping content was 1 at.%. The Mn^{2+} ion-related PL can be excited both at energies near the band-edge of ZnS host (the UV region) and at energies corresponding to the Mn^{2+} ion own excited states (the visible region). When the Mn-doped ZnS nanoclusters are excited by the interband transitions, the energy transfer from ZnS host to Mn^{2+} ion is carried out by the photogenerated carriers in the bands or the carriers thermally released from the DAP states into the bands.

Acknowledgement

This work is financially supported by Ministry of Science and Technology of Viet Nam (Contract No. 38/355/2008/HD-NDT for Task of Protocol with Israel and Project No 103.02.51.09 from NAFOSTED). The authors thank Kelvin Nanocharacterisation Centre, University of Glasgow, UK and Dr. Sam McFazdean for HRTEM measurement support. The authors also thank the members of Prof. Nozue's group, Osaka University for the diffuse reflection measurements.

References

[1] R.N. Bhargava, D. Gallagher, X. Hong, A. Nurmikko, Phys. Rev. Lett. 72 (1994) 416.
[2] R.N. Bhargava, D. Gallagher, T. Welker, J. Luminescence 60–61 (1994) 275.
[3] L. Levy, N. Feltin, D. Ingert, M.P. Pileni, Langmuir 15 (1999) 3386.
[4] G. Counio, T. Gacoin, J.P. Boilot, J. Phys. Chem. B 102 (1998) 5257.
[5] M.J. Tanaka, J. Luminescence 100 (2002) 163.
[6] M. Morita, D. Rau, H. Fujii, Y. Minami, S. Murakami, M. Baba, M. Yoshita, H. Akiyama, J. Luminescence 87–89 (2000) 478.
[7] P.V. Radovanovic, N.S. Norberg, K.E. McNally, D.R. Gamelin, J. Am. Chem. Soc. 124 (2002) 15192.
[8] D.J. Norris, Nan Yao, F.T. Charnock, T.A. Kennedy, Nano Letters 1 (2001) 3.
[9] L. Sangwook, S. Daegwon, L. Jongwon, K. Seontai, I.Y. Parka, W. Mi-Sook, Mater. Sci. Eng. B 103 (2003) 241.
[10] K. Jayanthi, S. Chawla, H. Chander, D. Haranath, Cryst. Res. Technol. 42 (2007) 976.
[11] Ping Yang, Mengkai Lu, Dong Xu, Duolong Yuan, Guangjun Zhou, Chem. Phys. Lett. 336 (2001) 76.
[12] G. Hajisalem, M. Maradi, N. Taghavinia, M. Houshiar, Nanotechnology 20 (2009) 095706.
[13] Subhajit Biswas, Soumitra Kar, Nanotechnology 19 (2008) 045710.
[14] R. Maity, K.K. Chattopadhyay, Nanotechnology 15 (2004) 812.
[15] H.C. Warad, S.C. Ghosh, B. Hemtanon, C. Thanachayanont, J. Dutta, Sci. Technol. Adv. Mater. 6 (2005) 296.
[16] Sameer Sapra, J. Nanda, A. Anand, S.V. Bhat, D.D. Sarma, J. Nanosci. Nanotech. 3 (2003) 392.
[17] B. Bhattacharjee, D. Ganguli, K. Iakoubovskii, A. Stesmans, S. Chaudhuri, Bull. Mater. Sci. 25 (2002) 175.
[18] Lixin Cao, Jiahua Zhang, Shanling Ren, Shihua Huang, Appl. Phys. Lett. 80 (2002) 4300.
[19] M. Tanaka, J. Qi, Y. Masumoto, J. Luminescence 87–89 (2000) 472.
[20] W. Chen, F. Su, G. Li, A.G. Joly, J.O. Malm, J.O. Bovin, J. Appl. Phys. 92 (2002) 1950.
[21] Shigeo Shionoya, William M. Yen (Eds.), Phosphor Handbook edited under the Auspices of Phospor Research Society, CRC Press, Boca Raton Boston London Newyork Washington D.C., 1999. pp. 763.
[22] B.E. Warren, X-ray Diffraction Dover publications, Inc, New York, 1990. p. 253.
[23] T. Kushida, Y. Tanaka, Y. Oka, Solid State Commun. 14 (1974) 617.
[24] Sameer Sapra, N. Shanthi, D.D. Sarma, Phys. Rev. B 66 (2002) 205202.
[25] J.I. Pankove, Optical Processes in Semiconductors, Prentice-Hall Inc., USA, 1971. 36.
[26] B.Y. Geng, X.W. Liu, Q.B. Du, X.W. Wei, L.D. Zhang, Appl. Phys. Lett. 88 (2006) 163104.
[27] L. Levy, J.F. Hochepied, M.P. Pileni, J. Phys. Chem. 100 (1996) 18322.
[28] S. Kar, S. Chaudhuri, J. Phys. Chem. B 109 (2005) 3298.
[29] S. Oda, H. Kukimoto, J. Luminescence 18–19 (1979) 829.
[30] J. Leeb, V. Gebhardt, G. Muller, D. Haarer, D. Su, M. Giersig, McMahon, L. Spanhel, J. Phys. Chem. B 103 (1999) 7839.
[31] S. Kar, S. Biswas, S. Chaudhuri, P.M.G. Nambissan, Nanotechnology 18 (2007) 220606.
[32] Qi Xiao, Chong Xiao, Opt. Mater. 31 (2008) 455.
[33] K. Sooklal, B.S. Cullum, S.M. Angel, C.J. Murphy, J. Phys. Chem. 100 (1996) 4551.
[34] D.G. Thomas, M. Gershenzon, F.A. Trumbore, Phys. Rev. 133 (1964) A269.
[35] M. Tanaka, Y. Masumoto, Chem. Phys. Lett. 324 (2000) 249.
[36] J.F. Suyver, S.F. Wuister, J.J. Kelly, A. Meijerink, Nano Lett. 1 (2001) 429.